

Nonleptonic two-body charmless B decays involving a tensor meson in the perturbative QCD approach

Zhi-Tian Zou, Xin Yu, and Cai-Dian Lü*

Institute of High Energy Physics and Theoretical Physics Center for Science Facilities, Chinese Academy of Sciences, Beijing 100049, People's Republic of China

(Received 25 March 2012; published 6 November 2012)

Two-body charmless hadronic B decays involving a light tensor meson in their final states are studied in the perturbative QCD approach based on k_T factorization. From our calculations, we find that the decay branching ratios for the color-allowed, tree-dominated decays $B \rightarrow a_2^0 \pi^+$ and $B \rightarrow a_2^- \pi^+$ are of orders 10^{-6} and 10^{-5} , respectively, while other color-suppressed, tree-dominated decays have very small branching ratios. In general, the branching ratios of most decays are in the range of 10^{-5} to 10^{-8} , which are bigger by 1 or 2 orders of magnitude than those predictions obtained in the Isgur-Scora-Grinstein-Wise II model and in the covariant light front approach, but consistent with recent experimental measurements and QCD factorization calculations. Since decays with a tensor meson emitted from vacuum are prohibited in naive factorization, the contributions of nonfactorizable and annihilation diagrams are very important to these decays, which are calculable in our perturbative QCD approach. We also give predictions for the direct CP asymmetries, some of which are large enough for the future experiments to measure. Because we consider the mixing between f_2 and f_2' , the decay rates are enhanced significantly for some decays involving f_2' mesons, even with a small mixing angle.

DOI: [10.1103/PhysRevD.86.094015](https://doi.org/10.1103/PhysRevD.86.094015)

PACS numbers: 13.25.Hw, 12.38.Bx

I. INTRODUCTION

In the quark model, all kinds of mesons are classified by their spin-parity quantum numbers, J^P . For example, $J^P = 0^-$ denotes pseudoscalar mesons, and $J^P = 2^+$ represents tensor mesons. The p -wave tensor mesons that we study in this paper include isovector mesons, $a_2(1320)$; isodoublet states, $K_2^*(1430)$; and two isosinglet mesons, $f_2(1270)$, $f_2'(1525)$ [1,2]. For these nine tensor mesons, both the orbital angular momentum and the total spin of their quarks are equal to 1. Because of the requirement of the Bose statistics of the tensor meson, the light-cone distribution amplitudes of tensor mesons are antisymmetric under the interchange of momentum fractions of the quark and antiquark in the flavor $SU(3)$ limit [3,4].

Recently, several experimental measurements about charmless B decay modes involving a light tensor meson (T) in their final states have been obtained [5–18]. These decays have been studied in the naive factorization approach [19–27], with which it can be easily shown that $\langle 0 | j^\mu | T \rangle = 0$, where j^μ is the $(V \pm A)$ or $(S \pm P)$ current [3,4,22,23]. The factorizable amplitude with a tensor meson emitted vanishes, so these decays are prohibited in the naive factorization approach. The branching ratios predicted in the naive factorization approach are too small compared with the experimental results, which implies the importance of nonfactorizable and annihilation-type contributions. The recent QCD factorization (QCDF) approach analysis [4] proved this. It is worth mentioning that the perturbative QCD (PQCD) approach [28,29] is

almost the only method for calculating these kinds of diagrams without fitting the experiments.

In this work, we shall study charmless $B_{u(d)} \rightarrow PT$ decays in the perturbative QCD approach based on the k_T factorization. Due to the heavy mass of the B meson, the two light mesons decayed from it are moving very fast in the rest frame of the B meson. The light quarks in the final-state mesons are all collinear, while the light spectator quark from the B meson is soft. Therefore, there must be a hard gluon to kick the light spectator quark in the B meson to form a fast-moving light meson. In this case, the hard process dominates the decay amplitude, which makes it perturbatively calculable. By keeping the transverse momentum of quarks, the endpoint singularity in the collinear factorization can be eliminated. A double logarithm appears in the QCD radiative corrections due to the additional energy scale introduced by the transverse momentum. By using the renormalization group equation, the double logarithm can be resummed to give the Sudakov factor, which effectively suppresses the endpoint contribution of the distribution amplitude of mesons in the small momentum region to make the perturbative calculation reliable. The annihilation diagrams can also be perturbatively calculated in the PQCD approach, which provides the dominant strong phase in B decays for the direct CP asymmetry [30]. Phenomenologically, the PQCD approach has successfully predicted the direct CP asymmetry in hadronic B decays [30] and the branching ratios of pure annihilation-type B decays [31].

This paper is organized as follows: In Sec. II, we present the formalism and wave functions of the B meson and the final-state mesons. Then, we perform the perturbative

*lucd@ihep.ac.cn

calculations for considered decay channels with the PQCD approach in Sec. III. The numerical results and phenomenological analysis are given in Sec. IV. Section V contains the main conclusions and a short summary. Finally, Appendix A contains input parameters and distribution amplitudes used in this paper, and Appendix B gives various functions that enter the factorization formulas in the PQCD approach.

II. FORMALISM AND WAVE FUNCTIONS

The related weak effective Hamiltonian H_{eff} [32] for charmless $b \rightarrow d(s)$ transitions can be written as

$$H_{\text{eff}} = \frac{G_F}{\sqrt{2}} \left\{ \sum_{i=1}^2 C_i(\mu) V_{ub}^* V_{ud} O_i^u(\mu) - V_{tb}^* V_{td} \sum_{j=3}^{10} C_j(\mu) O_j(\mu) \right\}, \quad (1)$$

where V_{ub} , V_{ud} , V_{tb} , and V_{td} are CKM matrix elements; D denotes the light down quark d or s ; and $C_{i(j)}(\mu)$ are Wilson coefficients at the renormalization scale μ . $O_{i(j)}(\mu)$ are the well-known effective tree (penguin) operators [32].

The nonleptonic B meson decays involve three energy scales, including the electroweak scale M_W , the b -quark mass scale M_B , and the factorization scale $\sqrt{\bar{\Lambda} M_B}$, where $\bar{\Lambda} \equiv M_B - m_b$. When the energy scale is higher than the W -boson mass M_W , the physics invoked is the electroweak interaction, which can be calculated perturbatively. The physics from the M_W scale to the M_B scale is described by the Wilson coefficients of effective four-quark operators, which is the resummation of the leading logarithm by renormalization equations. The physics between the M_B scale and the factorization scale is calculated by the hard part calculation in the PQCD approach. The physics below the factorization scale is described by the hadronic wave functions of mesons, which are nonperturbative but universal for all decay processes.

In the PQCD approach, the decay amplitude can be factorized into the convolution of the Wilson coefficients, the hard scattering kernel, and the light-cone wave functions of mesons characterized by the respective scales. Then, for $B \rightarrow M_2 M_3$ decays, the decay amplitude is conceptually written as the convolution

$$\mathcal{A} \sim \int dx_1 dx_2 dx_3 b_1 db_1 b_2 db_2 b_3 db_3 \text{Tr}[C(t) \Phi_B(x_1, b_1) \Phi_{M_2} \times (x_2, b_2) \Phi_{M_3}(x_3, b_3) H(x_i, b_i, t) S_t(x_i) e^{-S(t)}], \quad (2)$$

where x_i are the longitudinal momentum fractions of valence quarks, b_i are the conjugate space coordinates of the transverse momenta k_{iT} of the light quarks, and t is the largest scale in the function $H(x_i, b_i, t)$. By using the renormalization group equations, the large logarithms

$\ln(m_W/t)$ are included in the Wilson coefficients $C(t)$. By the threshold resummation, the large double logarithms $(\ln^2 x_i)$ are summed to give $S_t(x_i)$, which smears the endpoint singularities on x_i [33]. The last term, $e^{-S(t)}$, is the Sudakov factor, which suppresses the soft dynamics effectively [34]. Thus, it makes the perturbative calculation of the hard part H applicable at an intermediate scale, i.e., the m_B scale.

We will work in the B -meson rest frame and employ the light-cone coordinates for momentum variables. So the B -meson momentum is chosen as $P_1 = \frac{m_B}{\sqrt{2}}(1, 1, \mathbf{0}_T)$. For the nonleptonic charmless $B \rightarrow M_2 M_3$ decays, we assume that the $M_2(M_3)$ meson moves in the plus(minus) z direction carrying the momentum $P_2(P_3)$. Then the momenta are given by

$$P_2 = \frac{m_B}{\sqrt{2}}(1 - r_3^2, r_2^2, \mathbf{0}_T), \quad P_3 = \frac{m_B}{\sqrt{2}}(r_3^2, 1 - r_2^2, \mathbf{0}_T), \quad (3)$$

where $r_2 = \frac{m_{M_2}}{m_B}$ and $r_3 = \frac{m_{M_3}}{m_B}$. The (light) quark momenta in B , M_2 , and M_3 mesons are defined as k_1 , k_2 , and k_3 , respectively. We choose

$$k_1 = (x_1 P_1^+, 0, \mathbf{k}_{1T}), \quad k_2 = (x_2 P_2^+, 0, \mathbf{k}_{2T}), \quad (4)$$

$$k_3 = (0, x_3 P_3^-, \mathbf{k}_{3T}).$$

For a tensor meson, the polarization tensor $\epsilon_{\mu\nu}(\lambda)$ with helicity λ can be constructed via the polarization vectors of a vector meson [3,4]. They are given by

$$\epsilon^{\mu\nu}(\pm 2) \equiv \epsilon(\pm 1)^\mu \epsilon(\pm 1)^\nu,$$

$$\epsilon^{\mu\nu}(\pm 1) \equiv \sqrt{\frac{1}{2}} [\epsilon(\pm 1)^\mu \epsilon(0)^\nu + \epsilon(0)^\mu \epsilon(\pm 1)^\nu],$$

$$\epsilon^{\mu\nu}(0) \equiv \sqrt{\frac{1}{6}} [\epsilon(+1)^\mu \epsilon(-1)^\nu + \epsilon(-1)^\mu \epsilon(+1)^\nu] + \sqrt{\frac{2}{3}} \epsilon(0)^\mu \epsilon(0)^\nu. \quad (5)$$

With the tensor meson moving in the plus direction of the z axis, the polarization vectors of the vector meson are chosen as

$$\epsilon^\mu(0) = \frac{1}{\sqrt{2} m_T} (k_0 + k_3, k_0 - k_3, 0, 0), \quad (6)$$

$$\epsilon^\mu(\pm 1) = \frac{1}{\sqrt{2}} (0, 0, 1, \pm i),$$

where k_0 denotes the energy, and k_3 is the magnitude of the tensor meson momentum in the B -meson rest frame. The polarization tensor satisfies the relations [3,4]

$$\begin{aligned}\epsilon^{\mu\nu}(\lambda) &= \epsilon^{\nu\mu}(\lambda), & \epsilon_{\mu}^{\mu}(\lambda) &= 0, \\ \epsilon^{\mu\nu}(\lambda)P_{\mu} &= \epsilon^{\mu\nu}(\lambda)P_{\nu} = 0, & \epsilon_{\mu\nu}(\lambda)(\epsilon^{\mu\nu}(\lambda'))^* &= \delta_{\lambda\lambda'}.\end{aligned}\quad (7)$$

In the following calculation, we define a new polarization vector ϵ_T for the considered tensor meson for convenience [2]:

$$\epsilon_T(\lambda) = \frac{1}{m_B} \epsilon_{\mu\nu}(\lambda) P_B^{\nu}, \quad (8)$$

which satisfies

$$\begin{aligned}\epsilon_{T\mu}(\pm 2) &= 0, & \epsilon_{T\mu}(\pm 1) &= \frac{\epsilon(0) \cdot P_B \epsilon_{\mu}(\pm 1)}{\sqrt{2}m_B}, \\ \epsilon_{T\mu}(0) &= \frac{\sqrt{\frac{2}{3}}\epsilon(0) \cdot P_B \epsilon(0)}{m_B}.\end{aligned}\quad (9)$$

One can find that the new vector ϵ_T is similar to the polarization vector ϵ of a vector meson, regardless of the related constants [2].

In the PQCD approach, we should choose the proper wave functions for the B meson and light mesons to calculate the decay amplitude. Because the B meson is a pseudoscalar heavy meson, the two-structure ($\gamma_{\mu}\gamma_5$) and γ_5 components remain as leading contributions [2]. Thus, the B -meson wave function Φ_B is written as

$$\Phi_B = \frac{i}{\sqrt{6}} [(\not{P} + m_B)\gamma_5\phi_B(x)]. \quad (10)$$

For the distribution amplitude, we can choose

$$\phi_B(x, b) = N_B x^2 (1-x)^2 \exp\left[-\frac{1}{2}\left(\frac{m_B x}{\omega_B}\right)^2 - \frac{\omega_B^2 b^2}{2}\right], \quad (11)$$

where N_B is the normalization constant.

For the light pseudoscalar meson (P), the wave function is generally defined as

$$\Phi_P(x) = \frac{i}{\sqrt{6}} \gamma_5 \{ \not{P} \phi_P^A(x) + m_0^P \phi_P^P(x) + m_0^P (\not{P} - 1) \phi_P^T(x) \}, \quad (12)$$

where $\phi_P^{A,P,T}$ and m_0^P are the distribution amplitudes and chiral scale parameter of the pseudoscalar mesons, respectively. The variable x denotes the momentum fraction carried by the quark in the meson, and $n = (1, 0, \mathbf{0})$ and $v = (0, 1, \mathbf{0})$ are dimensionless lightlike unit vectors pointing in the plus and minus directions, respectively.

The wave functions for a generic tensor meson are defined by [2]

$$\begin{aligned}\Phi_T^L &= \frac{1}{\sqrt{6}} \left[m_T \epsilon_{\bullet L}^* \phi_T(x) + \epsilon_{\bullet L}^* \not{P} \phi_T^t(x) + m_T^2 \frac{\epsilon_{\bullet} \cdot v}{P \cdot v} \phi_T^s(x) \right], \\ \Phi_T^{\perp} &= \frac{1}{\sqrt{6}} \left[m_T \epsilon_{\bullet \perp}^* \phi_T^v(x) + \epsilon_{\bullet \perp}^* \not{P} \phi_T^T(x) \right. \\ &\quad \left. + m_T i \epsilon_{\mu\nu\rho\sigma} \gamma_5 \gamma^{\mu} \epsilon_{\bullet \perp}^{*\nu} n^{\rho} v^{\sigma} \phi_T^a(x) \right].\end{aligned}\quad (13)$$

Here n is the moving direction of the tensor meson, and v is the opposite direction. We adopt the convention $\epsilon^{0123} = 1$. The vector $\epsilon_{\bullet} \equiv \frac{\epsilon_{\mu\nu} v^{\nu}}{P \cdot v} m_T$ is related to the polarization tensor. The distribution amplitudes can be given by [2–4]

$$\begin{aligned}\phi_T(x) &= \frac{f_T}{2\sqrt{2}N_c} \phi_{\parallel}(x), & \phi_T^t(x) &= \frac{f_T^{\perp}}{2\sqrt{2}N_c} h_{\parallel}^{(t)}(x), \\ \phi_T^s(x) &= \frac{f_T^{\perp}}{4\sqrt{2}N_c} \frac{d}{dx} h_{\parallel}^{(s)}(x), & \phi_T^T(x) &= \frac{f_T^{\perp}}{2\sqrt{2}N_c} \phi_{\perp}(x), \\ \phi_T^v(x) &= \frac{f_T}{2\sqrt{2}N_c} g_{\perp}^{(v)}(x), & \phi_T^a(x) &= \frac{f_T}{8\sqrt{2}N_c} \frac{d}{dx} g_{\perp}^{(a)}(x).\end{aligned}\quad (14)$$

The asymptotic twist-2 distribution amplitude is given by

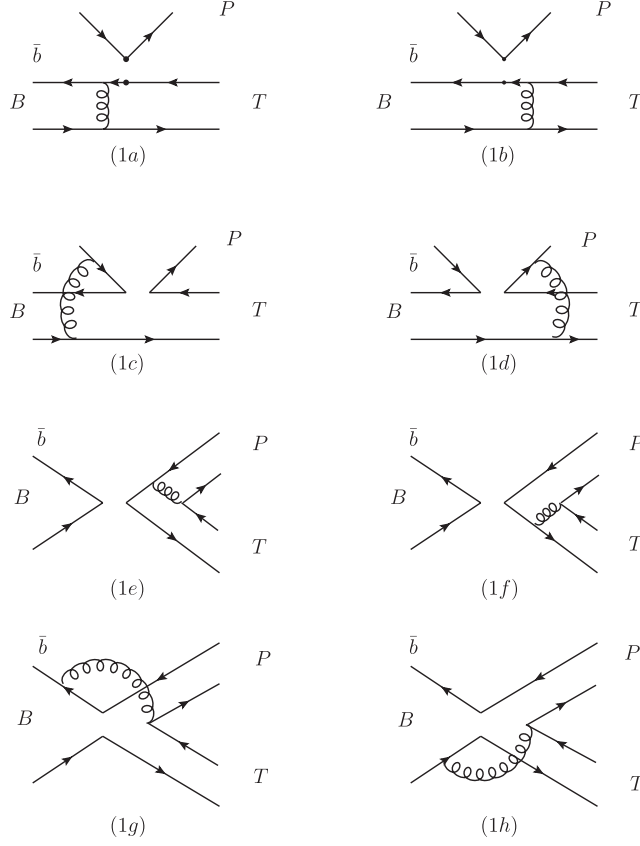
$$\phi_{\parallel, \perp}(x) = 30x(1-x)(2x-1). \quad (15)$$

The twist-3 distribution amplitudes are also asymptotic, and the forms are chosen as [2–4]

$$\begin{aligned}h_{\parallel}^{(t)}(x) &= \frac{15}{2}(2x-1)(1-6x+6x^2), \\ h_{\parallel}^{(s)}(x) &= 15x(1-x)(2x-1), \\ g_{\perp}^{(a)}(x) &= 20x(1-x)(2x-1), \\ g_{\perp}^{(v)}(x) &= 5(2x-1)^3.\end{aligned}\quad (16)$$

III. PERTURBATIVE CALCULATION

In this section, we will calculate the hard part $H(t)$, which includes the effective four-quark operators and the necessary hard gluon connecting the four quark-operator with the spectator quark [35]. There are eight types of diagrams contributing to the $B \rightarrow PT$ decays, shown in Fig. 1. From the first two diagrams, Figs. 1(a) and 1(b), by perturbative QCD calculations, we gain the decay amplitudes for factorizable emission contribution. For $(V-A)(V-A)$ current, the amplitude is written as

FIG. 1. Diagrams contributing to the $B \rightarrow PT$ decays, with a pseudoscalar meson emitted.

$$\begin{aligned} \mathcal{A}_{eT}^{LL} = & -8\sqrt{\frac{2}{3}}\pi C_F f_P M_B^4 \int_0^1 dx_1 dx_3 \int_0^\infty b_1 db_1 b_3 db_3 \phi_B(x_1, b_1) \{ [\phi_T(x_3)(x_3 + 1) - (\phi_T^s(x_3) \\ & + \phi_T^t(x_3))r_T(2x_3 - 1)] h_{ef}(x_1, x_3, b_1, b_3) E_{ef}(t_a) + [2r_T \phi_T^s(x_3)] h_{ef}(x_3, x_1, b_3, b_1) E_{ef}(t_b) \}, \end{aligned} \quad (17)$$

where $r_T = \frac{m_T}{m_B}$, $C_F = \frac{4}{3}$, and f_P is the decay constant of the pseudoscalar meson. The functions h_{ef} , $t_{a,b}$, and E_{ef} can be found in Appendix B. From Eq. (17), we can obtain the $\langle T|V - A|B \rangle$ transition form factor in the PQCD approach.

The operators O_5 , O_6 , O_7 , and O_8 have the structure $(V - A)(V + A)$. In some decay modes, some of these operators will contribute to the decay amplitude. Because only the axial part of $(V + A)$ current will contribute to the pseudoscalar meson production, we have

$$\mathcal{A}_{eT}^{LR} = -\mathcal{A}_{eT}^{LL}. \quad (18)$$

In some cases, in order to get the right color structure, we must do a Fierz transformation for these operators. So we obtain $(S - P)(S + P)$ operators from $(V - A)(V + A)$ ones. The decay amplitude is

$$\begin{aligned} \mathcal{A}_{eT}^{SP} = & 16\sqrt{\frac{2}{3}}C_F f_P \pi m_B^4 \int_0^1 dx_1 dx_3 \int_0^\infty b_1 db_1 b_3 db_3 \cdot \phi_B(x_1, b_1) \{ [\phi_T(x_3) + r_T(\phi_T^s(x_3)(x_3 + 2) \\ & - \phi_T^t(x_3)x_3)] r_0 h_{ef}(x_1, x_3, b_1, b_3) E_{ef}(t_a) + [2r_T r_0 \phi_T^s(x_3)] h_{ef}(x_3, x_1, b_3, b_1) E_{ef}(t_b) \}, \end{aligned} \quad (19)$$

where $r_0 = m_0^P/m_B$.

For the nonfactorizable diagrams in Figs. 1(c) and 1(d), the amplitudes involve all three wave functions. The integration of b_3 can be performed through the δ function $\delta(b_1 - b_3)$, leaving only the integration of b_1 and b_2 . For the $(V - A)(V - A)$, $(V - A)(V + A)$, and $(S - P)(S + P)$ -type operators, the amplitudes are

$$\begin{aligned} \mathcal{M}_{eT}^{LL} = & \frac{32}{3} C_F \pi m_B^4 \int_0^1 dx_1 dx_2 dx_3 \int_0^\infty b_1 db_1 b_2 db_2 \phi_B(x_1, b_1) \phi_P^A(x_2) \{ [\phi_T(x_3)(x_2 - 1) + (\phi_T^s(x_3) - \phi_T^l(x_3)) r_T x_3] \\ & \cdot h_{enf}(x_1, 1 - x_2, x_3, b_1, b_2) E_{enf}(t_c) + [\phi_T(x_3)(x_2 + x_3) - (\phi_T^s(x_3) + \phi_T^l(x_3)) r_T x_3] \cdot h_{enf}(x_1, x_2, x_3, b_1, b_2) E_{enf}(t_d) \}, \end{aligned} \quad (20)$$

$$\begin{aligned} \mathcal{M}_{eT}^{LR} = & -\frac{32}{3} C_F \pi r_0 m_B^4 \int_0^1 dx_1 dx_2 dx_3 \int_0^\infty b_1 db_1 b_2 db_2 \phi_B(x_1, b_1) \{ [\phi_P^T(x_2)(\phi_T(x_3)(x_2 - 1) + r_T(\phi_T^l(x_3)(-x_2 + x_3 + 1) \\ & + \phi_T^s(x_3)(x_2 + x_3 - 1))) + \phi_P^P(\phi_T(x_2 - 1) + r_T(\phi_T^s(x_3)(x_2 - x_3 - 1) - \phi_T^l(x_3)(x_2 + x_3 - 1)))] \\ & \cdot h_{enf}(x_1, 1 - x_2, x_3, b_1, b_2) E_{enf}(t_c) + [\phi_P^P(x_2)(\phi_T(x_3)x_2 + r_T(\phi_T^l(x_3)(x_3 - x_2) + \phi_T^s(x_3)(x_2 + x_3))) \\ & + \phi_P^T(r_T(\phi_T^s(x_3)(x_3 - x_2) + \phi_T^l(x_3)(x_2 + x_3)) - \phi_T(x_3)x_2)] \cdot h_{enf}(x_1, x_2, x_3, b_1, b_2) E_{enf}(t_d) \}, \end{aligned} \quad (21)$$

$$\begin{aligned} \mathcal{M}_{eT}^{SP} = & -\frac{32}{3} C_F \pi m_B^4 \int_0^1 dx_1 dx_2 dx_3 \int_0^\infty b_1 db_1 b_2 db_2 \phi_B(x_1, b_1) \phi_P^A(x_2) \{ [\phi_T(x_3)(x_2 - x_3 - 1) + (\phi_T^s(x_3) + \phi_T^l(x_3)) r_T x_3] \\ & \cdot h_{enf}(x_1, 1 - x_2, x_3, b_1, b_2) E_{enf}(t_c) + [\phi_T(x_3)x_2 + (\phi_T^l - \phi_T^s) r_T x_3] \cdot h_{enf}(x_1, x_2, x_3, b_1, b_2) E_{enf}(t_d) \}. \end{aligned} \quad (22)$$

Figures 1(e) and 1(f) give factorizable annihilation diagrams; the three kinds of decay amplitudes for these two diagrams are

$$\begin{aligned} \mathcal{A}_{aT}^{LL} = & 8\sqrt{\frac{2}{3}} C_F f_B \pi m_B^4 \int_0^1 dx_2 dx_3 \int_0^\infty b_2 db_2 b_3 db_3 \{ [2\phi_P^P(x_2) r_T r_0 (\phi_T^s(x_3)(x_3 - 2) - \phi_T^l(x_3)x_3) - \phi_P^A(x_2) \phi_T(x_3)(x_3 - 1)] \\ & \cdot h_{af}(x_2, 1 - x_3, b_2, b_3) E_{af}(t_e) + [2\phi_T^s(x_3) r_T r_0 (\phi_P^T(x_2)(x_2 - 1) + \phi_P^P(x_2)(x_2 + 1)) - \phi_P^A(x_2) \phi_T(x_3)x_2] \\ & \cdot h_{af}(1 - x_3, x_2, b_3, b_2) E_{af}(t_f) \}, \end{aligned} \quad (23)$$

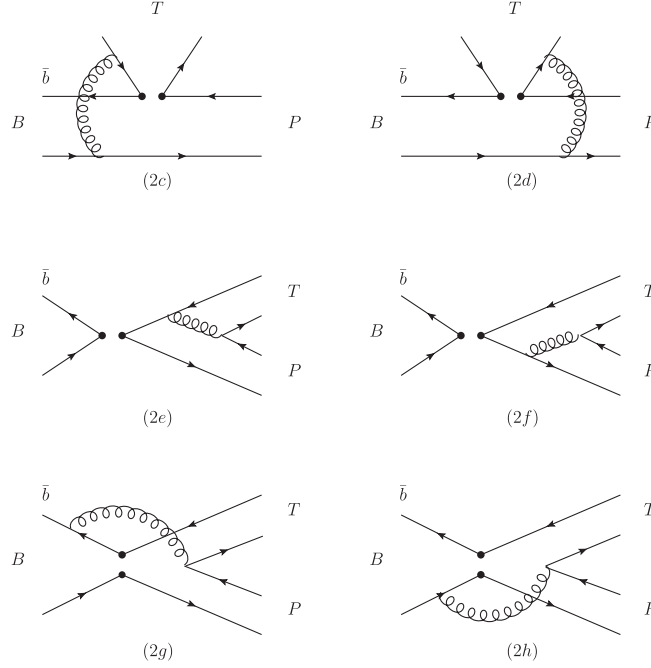
$$\mathcal{A}_{aT}^{LR} = -\mathcal{A}_{aT}^{LL}, \quad (24)$$

$$\begin{aligned} \mathcal{A}_{aT}^{SP} = & 16\sqrt{\frac{2}{3}} C_F f_B \pi m_B^4 \int_0^1 dx_2 dx_3 \int_0^\infty b_2 db_2 b_3 db_3 \{ [2\phi_P^P(x_2) \phi_T(x_3) r_0 + \phi_P^A(x_2)(\phi_T^s(x_3) + \phi_T^l(x_3)) r_T (x_3 - 1)] \\ & \cdot h_{af}(x_2, 1 - x_3, b_2, b_3) E_{af}(t_e) - [x_2 r_0 \phi_T(x_3)(\phi_P^T(x_2) - \phi_P^P(x_2)) + 2\phi_P^A(x_2) \phi_T^s(x_3) r_T] \cdot h_{af}(1 - x_3, x_2, b_3, b_2) E_{af}(t_f) \}. \end{aligned} \quad (25)$$

For the nonfactorizable annihilation diagrams in Figs. 1(g) and 1(h) all three wave functions are involved in the amplitudes. The integration of b_3 can be performed by the δ function $\delta(b_2 - b_3)$. The expressions of contributions for these two diagrams are

$$\begin{aligned} \mathcal{M}_{aT}^{LL} = & \frac{32}{3} C_F \pi m_B^4 \int_0^1 dx_1 dx_2 dx_3 \int_0^\infty b_1 db_1 b_2 db_2 \phi_B(x_1, b_1) \{ [-r_T r_0 (\phi_P^T(x_2)(\phi_T^s(x_3)(x_2 - 1 + x_3) - \phi_T^l(x_3)(x_2 - 1 - x_3)) \\ & + \phi_P^P(x_2)(\phi_T^l(x_3)(1 - x_2 - x_3) + \phi_T^s(x_3)(x_2 - x_3 + 3))) + \phi_P^A(x_2) \phi_T(x_3)x_2] \cdot h_{anf1}(x_1, x_2, x_3, b_1, b_2) E_{anf}(t_g) \\ & + [r_T r_0 (\phi_P^P(x_2)(\phi_T^s(x_3)(x_2 - x_3 + 1) + \phi_T^l(x_3)(x_2 + x_3 - 1)) - \phi_P^T(x_2)(\phi_T^l(x_3)(x_2 - x_3 + 1) + \phi_T^s(x_3)(x_2 + x_3 - 1))) \\ & + \phi_P^A(x_2) \phi_T(x_3)(x_3 - 1)] h_{anf2}(x_1, x_2, x_3, b_1, b_2) E_{anf}(t_h) \}, \end{aligned} \quad (26)$$

$$\begin{aligned} \mathcal{M}_{aT}^{LR} = & \frac{32}{3} C_F \pi m_B^4 \int_0^1 dx_1 dx_2 dx_3 \int_0^\infty b_1 db_1 b_2 db_2 \phi_B(x_1, b_1) \{ [r_T \phi_P^A(x_2)(\phi_T^s(x_3) - \phi_T^l(x_3))(x_3 + 1) \\ & - r_0 \phi_T(x_3)(\phi_P^P(x_2) + \phi_P^T(x_2)) \cdot (x_2 - 2)] h_{anf1}(x_1, x_2, x_3, b_1, b_2) E_{anf}(t_g) + [r_0 \phi_T(x_3)x_2(\phi_P^P(x_2) \\ & + \phi_P^T(x_2)) - r_T \phi_P^A(x_2)(\phi_T^s(x_3) - \phi_T^l(x_3))(x_3 - 1)] \cdot h_{anf2}(x_1, x_2, x_3, b_1, b_2) E_{anf}(t_h) \}, \end{aligned} \quad (27)$$

FIG. 2. Diagrams contributing to the $B \rightarrow PT$ decays, with a tensor meson emitted.

$$\begin{aligned}
\mathcal{M}_{aT}^{SP} = & \frac{32}{3} C_F \pi m_B^4 \int_0^1 dx_1 dx_2 dx_3 \int_0^\infty b_1 db_1 b_2 db_2 \phi_B(x_1, b_1) \{ [-r_T r_0 \phi_P^T(x_2) (\phi_T^s(x_3)(x_2 - 1 + x_3) + \phi_T^l(x_3)(x_2 - 1 - x_3)) \\
& + r_0 r_T \phi_P^P(x_2) (\phi_T^s(x_3)(x_2 - x_3 + 3) + \phi_T^l(x_3)(x_2 + x_3 - 1)) + \phi_P^A(x_2) \phi_T(x_3)(x_3 - 1)] h_{anf1}(x_1, x_2, x_3, b_1, b_2) E_{anf}(t_g) \\
& + [-r_0 r_T \phi_P^P(x_2) (\phi_T^s(x_3)(x_2 + 1 - x_3) + \phi_T^l(x_3)(1 - x_2 - x_3)) - r_0 r_T \phi_P^T(x_2) (\phi_T^l(x_3)(-x_2 + x_3 - 1) \\
& + \phi_T^s(x_3)(x_2 + x_3 - 1)) + \phi_P^A(x_2) \phi_T(x_3)x_2] h_{anf2}(x_1, x_2, x_3, b_1, b_2) E_{anf}(t_h) \}. \quad (28)
\end{aligned}$$

If we exchange the pseudoscalar meson and the tensor meson in Fig. 1, the result will be different. Because a tensor meson cannot be produced through $(V \pm A)$ or tensor current, the factorizable emission diagrams do not contribute to the amplitude of B decays with a tensor meson emitted [3,4]. Therefore, there are only six diagrams shown in Fig. 2. The individual decay amplitudes for these diagrams can be easily deduced from Eqs. (20)–(28) by the replacement of the wave functions of the pseudoscalar and the tensor meson:

$$\begin{aligned}
\phi_P^A(x) & \rightarrow -\phi_T(x), & \phi_P^P(x) & \rightarrow \phi_T^s(x), \\
\phi_P^T(x) & \rightarrow \phi_T^l(x), & \phi_T(x) & \rightarrow -\phi_P^A(x), \\
\phi_T^s(x) & \rightarrow -\phi_P^P(x), & \phi_T^l(x) & \rightarrow -\phi_P^T(x), \\
r_T & \rightarrow r_0, & r_0 & \rightarrow r_T.
\end{aligned} \quad (29)$$

In addition, we must add a minus sign to M_{eT}^{SP} after applying the above replacement.

For the 39 $B \rightarrow PT$ decay channels, not all the effective operators contribute to each decay mode. We list the number of effective operators contributing to the individual decay channels in Appendix B for reference.

IV. NUMERICAL RESULTS AND DISCUSSIONS

For the numerical analysis, we need various input parameters, such as decay constants, CKM elements, and the wave functions, which are given in Appendix A. The CP -averaged branching ratios for those $B \rightarrow PT$ decays with $\Delta S = 1$, together with the Isgur-Scora-Grinstein-Wise II (ISGW2) model [24] and the QCDF results [4] are shown in Table I. The experimental data are taken from Refs. [1,36]. Similarly, the branching ratios of $B \rightarrow PT$ decays with $\Delta S = 0$ calculated in the PQCD approach are shown in Table II. For illustration, we classify these decays by their dominant topologies, indicated through the symbols T (color-allowed tree), C (color-suppressed tree), P (penguin emission), and PA (penguin annihilation). Although we include also the W annihilation and W exchange diagram contributions, none of these channels has a dominant contribution from these two topologies. For the theoretical uncertainties in our calculation, we estimate three kinds of error: The first set of errors are caused by the uncertainties of the decay constants of tensor mesons. The second set of errors are from the decay constant $f_B = (0.21 \pm 0.02)$ GeV of the B meson and the shape parameter $\omega_B = (0.5 \pm 0.05)$ GeV in the B -meson wave

TABLE I. The PQCD predictions of CP -averaged branching ratios (in units of 10^{-6}) for $B \rightarrow PT$ decays with $\Delta S = 1$, together with the Isgur-Scora-Grinstein-Wise II (ISGW2) model [24] and QCDF results [4]. The experimental data are from Refs. [1,36].

Decay modes	Class	This work	ISGW2 [24]	QCDF [4]	Expt.
$B^+ \rightarrow K_2^{*0} \pi^+$	PA	$0.9^{+0.2+0.2+0.3}_{-0.2-0.2-0.2}$...	$3.1^{+8.3}_{-3.1}$	$5.6^{+2.2}_{-1.4}$
$B^+ \rightarrow K_2^{*+} \pi^0$	PA	$0.4^{+0.1+0.1+0.1}_{-0.0-0.1-0.1}$	0.090	$2.2^{+4.7}_{-1.9}$...
$B^+ \rightarrow a_2^0 K^+$	T, PA	$2.1^{+0.7+0.6+0.6}_{-0.6-0.5-0.5}$	0.31	$4.9^{+8.4}_{-4.2}$	<45
$B^+ \rightarrow a_2^+ K^0$	PA	$3.1^{+0.9+0.9+1.1}_{-0.8-0.8-0.9}$	0.011	$8.4^{+16.1}_{-7.2}$...
$B^+ \rightarrow f_2 K^+$	T, PA, P	$11.8^{+2.7+3.2+3.0}_{-2.4-2.8-2.7}$	0.34	$3.8^{+7.8}_{-3.0}$	$1.06^{+0.28}_{-0.29}$
$B^+ \rightarrow f' K^+$	P, PA	$3.8^{+0.4+0.9+1.0}_{-0.4-0.8-0.8}$	0.004	$4.0^{+7.4}_{-3.6}$	<7.7
$B^+ \rightarrow K_2^{*+} \eta$	PA, P	$0.8^{+0.2+0.3+0.3}_{-0.2-0.2-0.3}$	0.031	$6.8^{+13.5}_{-8.7}$	9.1 ± 3.0
$B^+ \rightarrow K_2^{*+} \eta'$	PA, P	$12.7^{+3.7+4.5+4.0}_{-3.2-3.5-3.5}$	1.41	$12.1^{+20.7}_{-12.1}$	$28.0^{+5.3}_{-5.0}$
$B^0 \rightarrow K_2^{*+} \pi^-$	PA	$1.0^{+0.2+0.2+0.3}_{-0.2-0.2-0.2}$...	$3.3^{+8.5}_{-3.2}$	<6.3
$B^0 \rightarrow K_2^{*0} \pi^0$	PA	$0.6^{+0.2+0.1+0.2}_{-0.1-0.1-0.1}$	0.084	$1.2^{+4.3}_{-1.3}$	<4.0
$B^0 \rightarrow a_2^- K^+$	T, PA	$5.0^{+1.6+1.4+1.3}_{-1.4-1.1-1.0}$	0.58	$9.7^{+17.2}_{-8.1}$...
$B^0 \rightarrow a_2^0 K^0$	PA	$2.0^{+0.5+0.4+0.6}_{-0.5-0.4-0.5}$	0.005	$4.2^{+8.3}_{-3.5}$...
$B^0 \rightarrow f_2 K^0$	PA, P	$9.2^{+2.0+2.5+2.6}_{-1.8-2.1-2.2}$	0.005	$3.4^{+8.5}_{-3.1}$	$2.7^{+1.3}_{-1.2}$
$B^0 \rightarrow f'_2 K^0$	P, PA	$3.7^{+0.3+0.7+0.9}_{-0.4-0.8-0.9}$	0.00007	$3.8^{+7.3}_{-3.5}$...
$B^0 \rightarrow K_2^{*0} \eta$	PA, P	$1.0^{+0.2+0.3+0.3}_{-0.2-0.2-0.3}$	0.029	$6.6^{+13.5}_{-8.7}$	9.6 ± 2.1
$B^0 \rightarrow K_2^{*0} \eta'$	PA, P	$11.6^{+3.6+4.2+3.8}_{-2.9-3.1-3.1}$	1.30	$12.4^{+21.3}_{-12.4}$	$13.7^{+3.2}_{-3.1}$

function [3,4,28,37]. The third set of errors are estimated from the unknown next-to-leading-order QCD corrections and the power corrections, characterized by the choice that $\Lambda_{\text{QCD}} = (0.25 \pm 0.05)$ GeV and the variations of the factorization scales shown in Appendix B, respectively. One can find that for most channels, the sizes of these three kinds of theoretical uncertainties are comparable.

There are large theoretical uncertainties in any of the individual decay mode calculations. However, we can reduce the uncertainties by ratios of decay channels. For example, simple relations among some decay channels are derived in the limit of $SU(3)$ flavor symmetry:

$$\begin{aligned}
\mathcal{B}(B^0 \rightarrow K_2^{*0} \pi^0) &\sim \mathcal{B}(B^+ \rightarrow K_2^{*+} \pi^0) \\
&\sim \frac{1}{2} \mathcal{B}(B^0 \rightarrow K_2^{*+} \pi^-) \sim \frac{1}{2} \mathcal{B}(B^+ \rightarrow K_2^{*0} \pi^+), \\
\frac{\mathcal{B}(B^0 \rightarrow a_2^- K^+)}{\mathcal{B}(B^+ \rightarrow a_2^0 K^+)} &= \frac{\mathcal{B}(B^+ \rightarrow a_2^+ K^0)}{\mathcal{B}(B^0 \rightarrow a_2^0 K^0)} = 2.
\end{aligned} \tag{30}$$

One can find that our results basically agree with the relation given above within the errors.

Among the considered $B \rightarrow PT$ decays, the PQCD predictions for the CP -averaged branching ratios vary in the range of 10^{-5} to 10^{-8} . From the numerical results, we can see that the predicted branching ratios of penguin-dominated $B \rightarrow PT$ decays in PQCD are larger than those of naive factorization [24,25,27] by 1 or 2 orders of magnitude, but are close to the QCDF predictions [4]. For the leading tree-dominated modes such as $a_2^- \pi^+$ and $f_2 \pi^+$, the

predicted results in PQCD are bigger than those obtained by QCDF [4] but smaller than those in Ref. [27]. The reason is that the B -to-tensor form factor in this work is larger than that used in Ref. [4]. For $a_2^0 \pi^+$, the result is not larger than, but the same as, that of Ref. [4]. This is the result of destructive interference from color-suppressed tree (C) topology. It is worth remarking that $B^0 \rightarrow K_2^{*+} K^-$ and $B^0 \rightarrow K_2^{*-} K^+$ are pure annihilation modes, which can be perturbatively calculated in the PQCD approach.

The decays with a tensor meson emitted are prohibited in the naive factorization approach for the reason that a tensor meson cannot be produced from the local ($V \pm A$) and tensor currents [3,4]. In order to predict these decay channels, it is necessary to go beyond the naive factorization framework to estimate the contributions of the nonfactorizable and annihilation diagrams. Fortunately, in the PQCD approach, the total contribution of the nonfactorizable diagrams with a tensor meson emitted [Figs. 2(c) and 2(d)] is sizable and larger than that of the nonfactorizable diagrams emitting a pseudoscalar meson [Figs. 1(c) and 1(d)]. The reason is that the asymmetry of the light-cone distribution amplitudes of the tensor meson makes the contributions from Figs. 2(c) and 2(d) strengthen with each other, while the situation is contrary for Figs. 1(c) and 1(d). One can see from Table II that for $B \rightarrow a_2 \pi$ decays, the $a_2^+ \pi^-$ and $a_2^+ \pi^0$ modes are highly suppressed relative to $a_2^- \pi^+$ and $a_2^0 \pi^+$, respectively. This is a natural consequence of factorization, as the tensor meson cannot be created from the ($V - A$) current. For $B \rightarrow a_2^0 \pi^+(a_2^- \pi^+)$, the dominant

TABLE II. The PQCD predictions of CP -averaged branching ratios (in units of 10^{-7}) for $B \rightarrow PT$ decays with $\Delta S = 0$, together with the Isgur-Scora-Grinstein-Wise II (ISGW2) model [24] and QCDF results [4]. The experimental data are from Refs. [1,36].

Decay modes	Class	This work	ISGW2 [24]	QCDF [4]	Expt.
$B^+ \rightarrow a_2^0 \pi^+$	T, C	$29.1^{+12.8+14.2+3.1}_{-10.6-10.4-2.8}$	26.02	30^{+14}_{-12}	...
$B^+ \rightarrow a_2^+ \pi^0$	T, C	$0.3^{+0.0+0.1+0.0}_{-0.0-0.1-0.0}$	0.01	$2.4^{+4.9}_{-3.1}$...
$B^+ \rightarrow a_2^+ \eta$	C, PA, P	$1.0^{+0.3+0.4+0.4}_{-0.3-0.3-0.3}$	2.94	$1.1^{+2.8}_{-1.1}$...
$B^+ \rightarrow a_2^+ \eta'$	C, PA, P	$3.5^{+1.4+1.6+1.1}_{-1.0-1.1-0.8}$	13.1	$1.1^{+4.7}_{-1.2}$...
$B^+ \rightarrow f_2 \pi^+$	T	$42.5^{+18.9+18.9+4.2}_{-15.4-13.9-3.9}$	28.74	27^{+14}_{-12}	$15.7^{+6.9}_{-4.9}$
$B^+ \rightarrow f_2' \pi^+$	T	$1.2^{+0.3+0.4+0.1}_{-0.2-0.3-0.1}$	0.37	$0.09^{+0.24}_{-0.09}$...
$B^+ \rightarrow K_2^{*+} \bar{K}^0$	PA, P	$1.2^{+0.2+0.2+0.3}_{-0.2-0.2-0.3}$	4.0×10^{-4}	$4.4^{+7.4}_{-4.1}$...
$B^+ \rightarrow \bar{K}_2^{*0} K^+$	PA	$0.8^{+0.1+0.2+0.3}_{-0.1-0.2-0.2}$...	$1.2^{+5.2}_{-1.2}$...
$B^0 \rightarrow a_2^- \pi^+$	T	$98.9^{+35.1+42.6+5.8}_{-29.9-32.0-9.7}$	48.82	52^{+18}_{-18}	<3000
$B^0 \rightarrow a_2^+ \pi^-$	T, PA	$2.7^{+0.5+0.8+0.4}_{-0.3-0.5-0.3}$...	$2.1^{+4.3}_{-1.7}$...
$B^0 \rightarrow a_2^0 \pi^0$	C	$4.6^{+1.2+1.6+0.9}_{-1.0-1.2-0.7}$	0.003	$2.4^{+4.2}_{-1.9}$...
$B^0 \rightarrow a_2^0 \eta$	C, PA, P	$0.6^{+0.1+0.2+0.1}_{-0.1-0.1-0.1}$	1.38	$0.6^{+1.6}_{-0.5}$...
$B^0 \rightarrow a_2^0 \eta'$	C, PA, P	$1.8^{+0.6+0.7+0.4}_{-0.5-0.6-0.4}$	6.15	$0.5^{+2.2}_{-0.4}$...
$B^0 \rightarrow f_2 \pi^0$	C	$2.8^{+0.7+0.7+0.6}_{-0.6-0.6-0.4}$	0.003	$1.5^{+4.2}_{-1.4}$...
$B^0 \rightarrow f_2' \pi^0$	P	$0.2^{+0.0+0.1+0.0}_{-0.0-0.1-0.0}$	4.0×10^{-5}	$0.05^{+0.12}_{-0.05}$...
$B^0 \rightarrow f_2 \eta$	C, P, PA	$2.6^{+0.7+0.8+0.7}_{-0.5-0.6-0.6}$	1.52	$1.7^{+2.3}_{-1.2}$...
$B^0 \rightarrow f_2 \eta'$	C, PA, P	$3.3^{+1.0+1.1+0.9}_{-0.8-0.9-0.9}$	6.8	$1.3^{+2.2}_{-1.3}$...
$B^0 \rightarrow f_2' \eta$	PA, P	$0.08^{+0.03+0.03+0.01}_{-0.02-0.03-0.02}$	0.02	$0.02^{+0.06}_{-0.03}$...
$B^0 \rightarrow f_2' \eta'$	PA, P	$0.09^{+0.00+0.02+0.02}_{-0.00-0.02-0.03}$	0.09	$0.08^{+0.08}_{-0.05}$...
$B^0 \rightarrow K_2^{*+} K^-$	PA	$0.16^{+0.02+0.03+0.03}_{-0.03-0.04-0.03}$...	$0.3^{+0.7}_{-0.2}$...
$B^0 \rightarrow K_2^{*-} K^+$	PA	$0.9^{+0.1+0.3+0.2}_{-0.1-0.1-0.2}$...	$1.3^{+1.6}_{-1.0}$...
$B^0 \rightarrow K_2^{*0} \bar{K}^0$	P, PA	$1.5^{+0.3+0.3+0.5}_{-0.3-0.3-0.4}$	3.0×10^{-4}	$5.4^{+8.8}_{-4.9}$...
$B^0 \rightarrow \bar{K}_2^{*0} K^0$	P, PA	$0.8^{+0.1+0.2+0.3}_{-0.1-0.1-0.2}$...	$2.2^{+5.4}_{-2.2}$...

contribution is from color-allowed factorizable emission diagrams, while for $B \rightarrow a_2^+ \pi^0 (a_2^+ \pi^-)$, this large contribution is prohibited for the above reason. Therefore, for $B^+ \rightarrow a_2^+ \pi^0$, the left factorizable emission diagrams are color suppressed, and for $B^0 \rightarrow a_2^+ \pi^-$, the dominant contribution is from nonfactorizable emission diagrams suppressed by the Wilson coefficient C_1 .

From Table VI, one can see that the factorizable contributions for the $B^+ \rightarrow K_2^{*0} \pi^+$ and $B^0 \rightarrow K_2^{*+} \pi^-$ decays are zero, because the emitted meson in these diagrams is the tensor meson. The contributions from nonfactorizable diagrams are suppressed by the small Wilson coefficients C_3 and C_5 . Therefore, the dominant contribution comes from the penguin annihilation diagrams. From Table I, one can see that our predictions for the $B^+ \rightarrow K_2^{*0} \pi^+$ and $B^0 \rightarrow K_2^{*+} \pi^-$ decays are much smaller than those of Ref. [4]. The reason is that in Ref. [4], there is an extremely large contribution from the quark loop diagrams. In the PQCD approach, the quark loop correction is next-to-leading order and not considered in this work. In the $B \rightarrow f_2 K$ decays, we have tree diagram contributions as

well as penguin emission diagram contributions, so the branching ratios are much larger than those of $B^+ \rightarrow K_2^{*0} \pi^+$ and $B^0 \rightarrow K_2^{*+} \pi^-$ decays. The current experimental measurements still have very large error bars. We expect future experiments to give more information for these decays.

For $B \rightarrow K_2^* \eta^{(\prime)}$ and $B \rightarrow a_2 \eta^{(\prime)}$ decays, one finds that $\mathcal{B}(B \rightarrow K_2^* \eta') \gg \mathcal{B}(B \rightarrow K_2^* \eta)$ and $\mathcal{B}(B \rightarrow a_2 \eta) \ll \mathcal{B}(B \rightarrow a_2 \eta')$. For these modes, both η_q and η_s will contribute, but the relative sign of the η_s state with respect to the η_q state is negative for η and positive for η' , which leads to destructive interference between η_q and η_s for $B \rightarrow K_2^* \eta$ and $B \rightarrow a_2 \eta$, but constructive interference for $B \rightarrow K_2^* \eta'$ and $B \rightarrow a_2 \eta'$. This is very similar to the situations for $B \rightarrow K \eta^{(\prime)}$ and $B_c \rightarrow K^+ \eta^{(\prime)}$ decays [38,39].

We also give the direct CP asymmetry parameters for those $B \rightarrow PT$ decays with $\Delta S = 1$, together with the QCDF results [4], in Table III. The experimental data are taken from Ref. [1]. Similarly, the direct CP asymmetry parameters of $B \rightarrow PT$ decays with $\Delta S = 0$ calculated in

TABLE III. The PQCD predictions of direct CP asymmetries (%) for $B \rightarrow PT$ decays with $\Delta S = 1$, compared with the QCDF results [4]. The experimental data are from Ref. [1].

Decay modes	This work	QCDF [4]	Expt.
$B^+ \rightarrow K_2^{*0} \pi^+$	$-5.5^{+0.3+2.6+1.6}_{-0.4-0.0-1.2}$	$1.6^{+2.2}_{-1.8}$	5^{+29}_{-24}
$B^+ \rightarrow K_2^{*+} \pi^0$	$-6.9^{+2.6+1.6+3.7}_{-2.9-1.1-3.6}$	$0.2^{+17.8}_{-14.8}$...
$B^+ \rightarrow a_2^0 K^+$	$-52.9^{+2.0+2.1+8.6}_{-2.2-0.4-10.1}$	$27.1^{+33.3}_{-35.0}$...
$B^+ \rightarrow a_2^+ K^0$	$2.9^{+0.1+0.1+0.5}_{-0.1-0.2-0.8}$	$-0.6^{+0.4}_{-0.8}$...
$B^+ \rightarrow f_2 K^+$	$-24.6^{+1.5+2.4+4.6}_{-1.0-2.6-5.9}$	$-39.5^{+49.4}_{-25.5}$	-68.0^{+19}_{-17}
$B^+ \rightarrow f' K^+$	$8.6^{+1.5+1.4+1.5}_{-1.6-1.0-1.8}$	$-0.6^{+4.3}_{-6.0}$...
$B^+ \rightarrow K_2^{*+} \eta$	$-5.4^{+1.1+2.2+2.3}_{-0.6-2.0-1.3}$	$1.5^{+7.4}_{-5.6}$	-45 ± 30
$B^+ \rightarrow K_2^{*+} \eta'$	$2.0^{+0.1+0.1+0.9}_{-0.1-0.3-0.5}$	$-1.7^{+3.2}_{-3.9}$...
$B^0 \rightarrow K_2^{*+} \pi^-$	$-17.5^{+1.4+1.6+2.7}_{-1.6-1.8-1.3}$	$1.7^{+4.2}_{-5.2}$...
$B^0 \rightarrow K_2^{*0} \pi^0$	$-10.7^{+0.1+1.7+1.9}_{-0.0-1.8-1.8}$	$7.1^{+23.5}_{-24.1}$...
$B^0 \rightarrow a_2^- K^+$	$-48.3^{+1.9+1.3+7.1}_{-2.4-0.3-9.9}$	$-21.5^{+28.9}_{-35.0}$...
$B^0 \rightarrow a_2^0 K^0$	$1.9^{+0.5+0.4+0.6}_{-0.5-0.4-0.5}$	$6.7^{+6.5}_{-6.9}$...
$B^0 \rightarrow f_2 K^0$	$1.2^{+0.3+0.5+0.2}_{-0.2-0.5-0.1}$	$-7.3^{+8.4}_{-7.9}$...
$B^0 \rightarrow f_2' K^0$	$-1.0^{+0.1+0.0+0.0}_{-0.3-0.1-0.1}$	$0.8^{+1.2}_{-0.7}$...
$B^0 \rightarrow K_2^{*0} \eta$	$-5.0^{+0.5+0.2+1.7}_{-0.4-0.1-1.7}$	$3.2^{+16.5}_{-4.8}$	-7.0 ± 19.0
$B^0 \rightarrow K_2^{*0} \eta'$	$0.7^{+0.1+0.1+0.3}_{-0.0-0.0-0.2}$	$-2.2^{+3.3}_{-4.0}$...

the PQCD approach are shown in Table IV. The origins of the theoretical uncertainties shown in these two tables are the same as those of the branching ratios in Tables I and II. However, the largest uncertainty here is the third one, from the unknown higher-order QCD corrections. The direct CP asymmetry is proportional to the strong phase originated from the hard part, and the higher-order QCD corrections of the hard part can influence the strong phase heavily. Therefore, the theoretical uncertainty caused by the unknown QCD corrections is larger than the first two errors from wave functions, which do not generate strong phase directly.

It is easy to see that some channels have very large direct CP asymmetries. But many of them have small branching ratios which are difficult to measure. We recommend that experimenters search for direct CP asymmetry in channels like $B^+ \rightarrow f_2 K^+$, $B^0 \rightarrow a_2^- K^+$, $B^+ \rightarrow a_2^+ \eta'$, and $B^+ \rightarrow f_2 \pi^+$, because they have both large branching ratios and direct CP asymmetry parameters. In fact, there are already some experimental measurements for the CP asymmetries shown in Tables III and IV. Although the error bars are still large, we are happy to see that all these measured entries have the same sign as our theoretical calculations. This may imply that our approach gives the dominant strong phase in these channels. The decays $B^0(\bar{B}^0) \rightarrow a_2^- \pi^+ / a_2^+ \pi^-$, $B^0(\bar{B}^0) \rightarrow K_2^{*+} K^- / K_2^{*-} K^+$, and $B^0(\bar{B}^0) \rightarrow K_2^{*0} \bar{K}^0 / \bar{K}_2^{*0} K^0$ have a very complicated CP pattern through the $B^0 \bar{B}^0$ mixing. Four decay amplitudes are involved for each group of decays, with five CP parameters to measure. We refer the readers to the similar situation for $B^0(\bar{B}^0) \rightarrow \rho^- \pi^+ / \rho^+ \pi^-$ decays [40].

For the decays involving $f_2^{(0)}$ in the final states, we have taken $f_2 - f_2'$ mixing [Eq. (A13)] into account, while in Ref. [4], f_2 is considered as an $(u\bar{u} + d\bar{d})/\sqrt{2}$ state and f_2' as a pure $s\bar{s}$ state. Although the mixing angle is small, the interference between f_2^q and f_2^s can bring some remarkable changes. For example, the branching ratio of $B^+ \rightarrow f_2' \pi^+$ is bigger than the prediction in Ref. [4]. This can be understood as follows: Because of the contribution from the color-allowed factorizable emission diagrams, although suppressed by the mixing angle, the contribution of f_2^q term is at the same level as that of f_2^s term. Due to the enhancement from the f_2^q term, the branching ratio becomes larger than the prediction without mixing. The mixing can also bring remarkable change to direct CP asymmetry. For $B \rightarrow f_2' \eta^{(0)}$, the direct CP asymmetries are zero [4] when f_2' is a pure $s\bar{s}$ state. Since the direct CP asymmetry is proportional to the interference between the tree and penguin contributions [30], it should be zero indeed, because there are no contributions of penguin operators when f_2' is a pure $s\bar{s}$ state. After taking the mixing into account, the f_2^q term can provide penguin contributions, and then the direct CP asymmetries are no longer zero in this work.

For $B \rightarrow f_2 \eta^{(0)}$ and $f_2' \eta^{(0)}$ decays, the relevant final-state mesons contain the same components, $\frac{1}{\sqrt{2}}(u\bar{u} + d\bar{d})$ and $s\bar{s}$; therefore they have similar branching ratios. The small differences among their branching ratios mainly come from different mixing coefficients; i.e., $\cos\phi$, $\sin\phi$, $\cos\theta$, and $\sin\theta$ (see Appendix A).

TABLE IV. The PQCD predictions of direct CP asymmetries (%) for $B \rightarrow PT$ decays with $\Delta S = 0$, compared with the QCDF results [4]. The experimental data are from Ref. [1].

Decay modes	This work	QCDF [4]	Expt.
$B^+ \rightarrow a_2^0 \pi^+$	$-0.6^{+0.1+0.4+0.2}_{-0.1-0.5-0.6}$	$9.6^{+47.9}_{-46.6}$...
$B^+ \rightarrow a_2^+ \pi^0$	$-5.8^{+0.1+21.3+75.8}_{-0.1-12.4-44.7}$	$-24.3^{+124.3}_{-75.7}$...
$B^+ \rightarrow a_2^+ \eta$	$-90.9^{+8.4+9.6+12.3}_{-3.7-1.0-5.1}$	$27.6^{+73.4}_{-127.6}$...
$B^+ \rightarrow a_2^+ \eta'$	$-44.5^{+0.8+1.3+6.8}_{-0.5-0.2-8.8}$	$31.3^{+61.3}_{-131.3}$...
$B^+ \rightarrow f_2 \pi^+$	$27.6^{+3.4+1.0+8.9}_{-2.5-1.4-7.1}$	$60.2^{+27.1}_{-72.3}$	41 ± 30
$B^+ \rightarrow f_2' \pi^+$	$0.03^{+0.1+9.6+13.8}_{-0.1-8.9-15.8}$	0.0	...
$B^+ \rightarrow K_2^{*+} \bar{K}^0$	$-43.7^{+1.3+1.8+16.4}_{-2.0-0.5-12.4}$	$30.3^{+51.2}_{-33.7}$...
$B^+ \rightarrow \bar{K}_2^{*0} K^+$	$49.5^{+4.7+3.1+23.5}_{-4.2-4.8-13.1}$	$-0.26^{+0.23}_{-0.27}$...
$B^0 \rightarrow a_2^0 \pi^0$	$53.5^{+4.7+6.9+4.2}_{-3.8-6.9-3.5}$	$-86.2^{+128.9}_{-26.4}$...
$B^0 \rightarrow a_2^0 \eta$	$-17.7^{+17.7+11.2+21.8}_{-15.7-22.6-24.5}$	$-76.7^{+100}_{-19.2}$...
$B^0 \rightarrow a_2^0 \eta'$	$-59.9^{+0.6+10.0+7.2}_{-0.0-6.0-7.0}$	$-66.0^{+154}_{-41.1}$...
$B^0 \rightarrow f_2 \pi^0$	$-9.8^{+13.9+2.8+11.8}_{-13.2-7.5-10.8}$	$-37.2^{+103.8}_{-85.5}$...
$B^0 \rightarrow f_2' \pi^0$	$-0.7^{+2.7+1.0+6.8}_{-2.5-1.8-6.4}$	0.0	...
$B^0 \rightarrow f_2 \eta$	$-42.5^{+1.7+1.4+9.1}_{-1.1-1.8-9.8}$	$69.7^{+25.7}_{-102.7}$...
$B^0 \rightarrow f_2 \eta'$	$-0.05^{+0.1+5.0+5.3}_{-0.6-5.1-5.3}$	$82.3^{+22.9}_{-94.8}$...
$B^0 \rightarrow f_2' \eta$	$70.9^{+0.0+11.0+11.0}_{-2.7-15.2-12.3}$	0.0	...
$B^0 \rightarrow f_2' \eta'$	$45.5^{+3.2+13.5+18.5}_{-6.8-12.1-18.8}$	0.0	...

V. SUMMARY

We studied charmless hadronic $B \rightarrow PT$ decays by employing the PQCD approach based on k_T factorization. In addition to the usual factorization contributions, we also calculated the nonfactorizable and annihilation type diagrams. From our numerical calculation and phenomenological analysis, we found the following results:

- The factorizable amplitude with a tensor meson emitted vanishes because a tensor meson cannot be created from the $(V \pm A)$ currents or $(S \pm P)$ density. The nonfactorizable and annihilation diagram contributions are important in these decay modes. For example, $B^+ \rightarrow K_2^{*0} \pi^+$ and $B^0 \rightarrow K_2^{*+} \pi^-$ have sizable branching ratios because of the contributions of penguin annihilation diagrams.
- For penguin-dominated $B \rightarrow PT$ decays, because of the dynamical penguin enhancement, the predicted branching ratios are larger by 1 or 2 orders of magnitude than those predicted in the naive factorization approach but close to the QCD factorization predictions in Ref. [4].
- For tree-dominated decay modes, the branching ratios predicted by PQCD are usually very small except for $a_2^0 \pi^+$, $a_2^- \pi^+$, and $f_2 \pi^+$ modes with branching ratios of order 10^{-6} or even larger. This basically agrees with the situations in Refs. [4,27].
- For $B \rightarrow K_2^* \eta^{(\prime)}$ decays, we find $\mathcal{B}(B \rightarrow K_2^* \eta^{(\prime)}) \gg \mathcal{B}(B \rightarrow K_2^* \eta)$. This large difference can be

explained by the destructive or constructive interference between η_q and η_s .

- The interference between f_2^q and f_2^s can bring remarkable effects to some decays involving a f_2' meson in branching-ratio and direct CP asymmetry.
- We predict large direct CP asymmetries for some of the $B \rightarrow PT$ decays that are accessible to near-future experiments.

ACKNOWLEDGMENTS

We are very grateful to Xin Liu and Wei Wang for helpful discussions. This work is partially supported by the National Science Foundation of China under Grants No. 11228512, No. 11235005, and No. 11075168.

APPENDIX A: INPUT PARAMETERS AND DISTRIBUTION AMPLITUDES

The masses and decay constants of tensor mesons are summarized in Table V. Other input parameters are

TABLE V. The masses and decay constants of light tensor mesons.

Tensor (mass in MeV)	f_T (MeV)	f_T^\perp (MeV)
$f_2(1270)$	102 ± 6	117 ± 25
$f_2'(1525)$	126 ± 4	65 ± 12
$a_2(1320)$	107 ± 6	105 ± 21
$K_2^*(1430)$	118 ± 5	77 ± 14

$$\Lambda_{\overline{MS}}^{f=A} = 0.25, \quad m_b = 4.8, \quad f_\pi = 0.131, \quad f_K = 0.16, \\ m_0^\pi = 1.4, \quad m_0^K = 1.6, \quad m_0^{\eta_q} = 1.07, \quad m_0^{\eta_s} = 1.92. \quad (\text{A1})$$

We adopt the Wolfenstein parameterization for the CKM matrix with $A = 0.808$, $\lambda = 0.2253$, $\bar{\rho} = 0.132$, and $\bar{\eta} = 0.341$ [1].

The twist-2(3) pseudoscalar meson distribution amplitude(s) $\phi_P^A(\phi_P^P, \phi_P^T)$ ($P = \pi, K$) can be parameterized as [41,42],

$$\phi_\pi^A(x) = \frac{3f_\pi}{\sqrt{6}}x(1-x)[1 + 0.44C_2^{3/2}(t) + 0.25C_4^{3/2}(t)], \quad (\text{A2})$$

$$\phi_\pi^P(x) = \frac{f_\pi}{2\sqrt{6}}[1 + 0.43C_2^{1/2}(t) + 0.09C_4^{1/2}(t)], \quad (\text{A3})$$

$$\phi_\pi^T(x) = -\frac{f_\pi}{2\sqrt{6}}[C_1^{1/2}(t) + 0.55C_3^{1/2}(t)], \quad (\text{A4})$$

$$\phi_K^A(x) = \frac{3f_K}{\sqrt{6}}x(1-x)[1 + 0.17C_1^{3/2}(t) + 0.2C_2^{3/2}(t)], \quad (\text{A5})$$

$$\phi_K^P(x) = \frac{f_K}{2\sqrt{6}}[1 + 0.24C_2^{1/2}(t) - 0.11C_4^{1/2}(t)], \quad (\text{A6})$$

$$\phi_K^T(x) = -\frac{f_K}{2\sqrt{6}}[C_1^{1/2}(t) + 0.35C_3^{1/2}(t)]. \quad (\text{A7})$$

The Gegenbauer polynomials can be defined as

$$C_1^{1/2}(t) = t, \quad C_1^{3/2}(t) = 3t, \\ C_2^{1/2}(t) = \frac{1}{2}(3t^2 - 1), \\ C_2^{3/2}(t) = \frac{3}{2}(5t^2 - 1), \\ C_3^{1/2}(t) = \frac{1}{2}t(5t^2 - 3), \\ C_4^{1/2}(t) = \frac{1}{8}(35t^4 - 30t^2 + 3), \\ C_4^{3/2}(t) = \frac{15}{8}(21t^4 - 14t^2 + 1), \quad (\text{A8})$$

where $t = 2x - 1$. In the above distribution amplitudes for the kaon, the momentum fraction x is carried by the s quark.

For the $\eta - \eta'$ system, we use the quark flavor basis [43], with η_q and η_s defined by

$$\eta_q = \frac{1}{\sqrt{2}}(u\bar{u} + d\bar{d}), \quad \eta_s = s\bar{s}. \quad (\text{A9})$$

The physical states η and η' can be given by

$$\begin{pmatrix} \eta \\ \eta' \end{pmatrix} = \begin{pmatrix} \cos\phi & -\sin\phi \\ \sin\phi & \cos\phi \end{pmatrix} \begin{pmatrix} \eta_q \\ \eta_s \end{pmatrix}. \quad (\text{A10})$$

The decay constants are related to f_q and f_s via the same mixing matrix:

$$\begin{pmatrix} f_\eta^q & f_\eta^s \\ f_{\eta'}^q & f_{\eta'}^s \end{pmatrix} = \begin{pmatrix} \cos\phi & -\sin\phi \\ \sin\phi & \cos\phi \end{pmatrix} \begin{pmatrix} f_q & 0 \\ 0 & f_s \end{pmatrix}. \quad (\text{A11})$$

The three input parameters f_q , f_s , and ϕ have been extracted from related experiments [43,44]:

$$f_q = (1.07 \pm 0.02)f_\pi, \quad f_s = (1.34 \pm 0.06)f_\pi, \\ \phi = 39.3^\circ \pm 1.0^\circ. \quad (\text{A12})$$

As with $\eta - \eta'$ mixing, the isoscalar tensor states $f_2(1270)$ and $f_2'(1525)$ also have a similar mixing:

$$f_2 = f_2^q \cos\theta + f_2^s \sin\theta, \quad f_2' = f_2^q \sin\theta - f_2^s \cos\theta, \quad (\text{A13})$$

where $f_2^q = \frac{1}{\sqrt{2}}(u\bar{u} + d\bar{d})$, $f_2^s = s\bar{s}$, and the mixing angle $\theta = 5.8^\circ$ [45], 7.8° [46], or $(9 \pm 1)^\circ$ [1].

APPENDIX B: AMPLITUDE AND RELATED HARD FUNCTIONS

For each individual decay channel, various effective operators contribute to the decay amplitude. We summarize the number of effective operators contributing to every channel in Tables VI and VII for $\Delta S = 1$ and $\Delta S = 0$, respectively, with

$$a_1 = \frac{C_1}{3} + C_2, \quad a_2 = C_1 + \frac{C_2}{3}, \\ a_j = C_j + \frac{C_{j+1}}{3} \quad (j = 3, 5, 7, 9), \\ a_n = \frac{C_{n-1}}{3} + C_n \quad (n = 4, 6, 8, 10). \quad (\text{B1})$$

For factorizable emission diagrams [Figs. 1(a) and 1(b)], the h function is given by

$$h_{ef}(x_1, x_3, b_1, b_3) \\ = K_0(\sqrt{x_1 x_3} m_B b_1) \{ \theta(b_1 - b_3) K_0(\sqrt{x_3} m_B b_1) I_0(\sqrt{x_3} m_B b_3) \\ + \theta(b_3 - b_1) K_0(\sqrt{x_3} m_B b_3) I_0(\sqrt{x_3} m_B b_1) \} S_t(x_3). \quad (\text{B2})$$

The hard scales

$$t_a = \max\{\sqrt{x_3} m_B, 1/b_1, 1/b_3\}, \\ t_b = \max\{\sqrt{x_1} m_B, 1/b_1, 1/b_3\} \quad (\text{B3})$$

are the maximum energy scales in each diagram to cancel the large logarithmic radiative corrections. The factor S_t resums the threshold logarithms $\ln^2 x$ in the hard kernels to all orders, as given by [33]

TABLE VI. The effective operators contributing to each decay mode with $\Delta S = 1$.

Channels	Emission		Annihilation	
	Factorizable	Nonfactorizable	Factorizable	Nonfactorizable
$B^0 \rightarrow K_2^{*+} \pi^-$	\dots	C_1, C_3, C_5, C_7, C_9	a_4, a_6, a_8, a_{10}	C_3, C_5, C_7, C_9
$B^0 \rightarrow a_2^- K^+$	$a_1, a_4, a_6, a_8, a_{10}$	C_1, C_3, C_5, C_7, C_9	a_4, a_6, a_8, a_{10}	C_3, C_5, C_7, C_9
$B^0 \rightarrow a_2^0 K^0$	a_4, a_6, a_8, a_{10}	$C_2, C_3, C_5, C_7, C_8, C_9, C_{10}$	a_4, a_6, a_8, a_{10}	C_3, C_5, C_7, C_9
$B^0 \rightarrow K_2^{*0} \pi^0$	a_2, a_7, a_9	$C_2, C_3, C_5, C_7, C_8, C_9, C_{10}$	a_4, a_6, a_8, a_{10}	C_3, C_5, C_7, C_9
$B^0 \rightarrow f_2^q K^0$	a_4, a_6, a_8, a_{10}	$C_2, C_3, C_4, C_5, C_6, C_7, C_8, C_9, C_{10}$	a_4, a_6, a_8, a_{10}	C_3, C_5, C_7, C_9
$B^0 \rightarrow \eta^q K_2^{*0}$	a_2, a_3, a_5, a_7, a_9	$C_2, C_3, C_4, C_5, C_6, C_7, C_8, C_9, C_{10}$	a_4, a_6, a_8, a_{10}	C_3, C_5, C_7, C_9
$B^0 \rightarrow f_2^s K^0$	\dots	$C_3, C_4, C_5, C_6, C_7, C_8, C_9, C_{10}$	a_4, a_6, a_8, a_{10}	C_3, C_5, C_7, C_9
$B^0 \rightarrow \eta^s K_2^{*0}$	$a_3, a_4, a_5, a_6, a_7, a_8, a_9, a_{10}$	$C_3, C_4, C_5, C_6, C_7, C_8, C_9, C_{10}$	a_4, a_6, a_8, a_{10}	C_3, C_5, C_7, C_9
$B^+ \rightarrow K_2^{*0} \pi^+$	\dots	C_3, C_5, C_7, C_9	$a_1, a_4, a_6, a_8, a_{10}$	C_1, C_3, C_5, C_7, C_9
$B^+ \rightarrow K^0 a_2^+$	a_4, a_6, a_8, a_{10}	C_3, C_5, C_7, C_9	$a_1, a_4, a_6, a_8, a_{10}$	C_1, C_3, C_5, C_7, C_9
$B^+ \rightarrow K_2^{*+} \pi^0$	a_2, a_7, a_9	$C_1, C_2, C_3, C_5, C_7, C_8, C_9, C_{10}$	$a_1, a_4, a_6, a_8, a_{10}$	C_1, C_3, C_5, C_7, C_9
$B^+ \rightarrow K^+ a_2^0$	$a_1, a_4, a_6, a_8, a_{10}$	$C_1, C_2, C_3, C_5, C_7, C_8, C_9, C_{10}$	$a_1, a_4, a_6, a_8, a_{10}$	C_1, C_3, C_5, C_7, C_9
$B^+ \rightarrow K^+ f_2^q$	$a_1, a_4, a_6, a_8, a_{10}$	$C_1, C_2, C_3, C_4, C_5, C_6, C_7, C_8, C_9, C_{10}$	$a_1, a_4, a_6, a_8, a_{10}$	C_1, C_3, C_5, C_7, C_9
$B^+ \rightarrow K_2^{*+} \eta^q$	a_2, a_3, a_5, a_7, a_9	$C_1, C_2, C_3, C_4, C_5, C_6, C_7, C_8, C_9, C_{10}$	$a_1, a_4, a_6, a_8, a_{10}$	C_1, C_3, C_5, C_7, C_9
$B^+ \rightarrow f_2^s K^+$	\dots	$C_3, C_4, C_5, C_6, C_7, C_8, C_9, C_{10}$	$a_1, a_4, a_6, a_8, a_{10}$	C_1, C_3, C_5, C_7, C_9
$B^+ \rightarrow \eta^s K_2^{*+}$	$a_3, a_4, a_5, a_6, a_7, a_8, a_9, a_{10}$	$C_3, C_4, C_5, C_6, C_7, C_8, C_9, C_{10}$	$a_1, a_4, a_6, a_8, a_{10}$	C_1, C_3, C_5, C_7, C_9

$$S_t(x) = \frac{2^{1+2c}\Gamma(3/2+c)}{\sqrt{\pi}\Gamma(1+c)} [x(1-x)]^c, \quad (\text{B4})$$

with $c = 0.3$ in this work. In the nonfactorizable contributions, $S_t(x)$ provides a very small numerical effect to the amplitude [47]. Therefore, we omit $S_t(x)$ in those contributions.

The evolution factors $E_{ef}(t_a)$ and $E_{ef}(t_b)$ in the matrix elements (see Sec. III) are given by

$$E_{ef}(t) = \alpha_s(t) \exp[-S_B(t) - S_3(t)]. \quad (\text{B5})$$

The Sudakov exponents are defined as

$$S_B(t) = s\left(x_1 \frac{m_B}{\sqrt{2}}, b_1\right) + \frac{5}{3} \int_{1/b_1}^t \frac{d\bar{\mu}}{\bar{\mu}} \gamma_q(\alpha_s(\bar{\mu})), \quad (\text{B6})$$

$$S_2(t) = s\left(x_2 \frac{m_B}{\sqrt{2}}, b_2\right) + s\left((1-x_2) \frac{m_B}{\sqrt{2}}, b_2\right) + 2 \int_{1/b_2}^t \frac{d\bar{\mu}}{\bar{\mu}} \gamma_q(\alpha_s(\bar{\mu})), \quad (\text{B7})$$

$$S_3(t) = s\left(x_3 \frac{m_B}{\sqrt{2}}, b_3\right) + s\left((1-x_3) \frac{m_B}{\sqrt{2}}, b_3\right) + 2 \int_{1/b_3}^t \frac{d\bar{\mu}}{\bar{\mu}} \gamma_q(\alpha_s(\bar{\mu})), \quad (\text{B8})$$

where $s(Q, b)$ can be found in Appendix A of Ref. [29].

For the other diagrams, the related functions are summarized as follows:

$$t_c = \max\{\sqrt{x_1 x_3} m_B, \sqrt{|1-x_1-x_2| x_3} m_B, 1/b_1, 1/b_2\},$$

$$t_d = \max\{\sqrt{x_1 x_3} m_B, \sqrt{|x_1-x_2| x_3} m_B, 1/b_1, 1/b_2\}, \quad (\text{B9})$$

$$E_{enf}(t) = \alpha_s(t) \cdot \exp[-S_B(t) - S_2(t) - S_3(t)]|_{b_1=b_3}, \quad (\text{B10})$$

$$h_{enf}(x_1, x_2, x_3, b_1, b_2) = [\theta(b_2 - b_1) K_0(\sqrt{x_1 x_3} m_B b_2) I_0(\sqrt{x_1 x_3} m_B b_1) + \theta(b_1 - b_2) K_0(\sqrt{x_1 x_3} m_B b_1) I_0(\sqrt{x_1 x_3} m_B b_2)] \cdot \begin{cases} \frac{i\pi}{2} H_0^{(1)}(\sqrt{(x_2 - x_1) x_3} m_B b_2), & x_2 - x_1 > 0; \\ K_0(\sqrt{(x_1 - x_2) x_3} m_B b_2), & x_1 - x_2 > 0. \end{cases} \quad (\text{B11})$$

$$t_e = \max\{\sqrt{1-x_3} m_B, 1/b_2, 1/b_3\},$$

$$t_f = \max\{\sqrt{x_2} m_B, 1/b_2, 1/b_3\}, \quad (\text{B12})$$

$$E_{af}(t) = \alpha_s(t) \cdot \exp[-S_2(t) - S_3(t)], \quad (\text{B13})$$

$$h_{af}(x_2, x_3, b_2, b_3) = \left(\frac{i\pi}{2}\right)^2 H_0^{(1)}(\sqrt{x_2 x_3} m_B b_2) [\theta(b_2 - b_3) H_0^{(1)}(\sqrt{x_3} m_B b_2) J_0(\sqrt{x_3} m_B b_3) + \theta(b_3 - b_2) H_0^{(1)}(\sqrt{x_3} m_B b_3) J_0(\sqrt{x_3} m_B b_2)] \cdot S_t(x_3). \quad (\text{B14})$$

$$t_g = \max\{\sqrt{x_2(1-x_3)} m_B, \sqrt{1-(1-x_1-x_2)} m_B, 1/b_1, 1/b_2\}$$

$$t_h = \max\{\sqrt{x_2(1-x_3)} m_B, \sqrt{|x_1-x_2|(1-x_3)} m_B, 1/b_1, 1/b_2\}, \quad (\text{B15})$$

$$E_{anf} = \alpha_s(t) \cdot \exp[-S_B(t) - S_2(t) - S_3(t)]|_{b_2=b_3}, \quad (\text{B16})$$

TABLE VII. The effective operators contributing to each decay mode with $\Delta S = 0$.

Channels	Emission		Annihilation	
	Factorizable	Nonfactorizable	Factorizable	Nonfactorizable
$B^0 \rightarrow f_2^q \pi^0$	$a_2, a_4, a_6, a_7,$ a_8, a_9, a_{10}	$C_2, C_3, C_4, C_5, C_6,$ C_7, C_8, C_9, C_{10}	$a_2, a_4, a_6, a_7, a_8,$ a_9, a_{10}	$C_2, C_3, C_5, C_7, C_8,$ C_9, C_{10}
$B^0 \rightarrow \eta^q a_2^0$	$a_2, a_3, a_4, a_5, a_6,$ a_7, a_8, a_9, a_{10}	$C_2, C_3, C_4, C_5, C_6,$ C_7, C_8, C_9, C_{10}	$a_2, a_4, a_6, a_7, a_8,$ a_9, a_{10}	$C_2, C_3, C_5, C_7, C_8,$ C_9, C_{10}
$B^0 \rightarrow a_2^- \pi^+$	$a_1, a_4, a_6, a_8, a_{10}$	C_1, C_3, C_5, C_7, C_9	$a_2, a_3, a_4, a_5, a_6,$ $a_7, 8, a_9, a_{10}$	$C_2, C_3, C_4, C_5, C_6,$ C_7, C_8, C_9, C_{10}
$B^0 \rightarrow \pi^- a_2^+$	\dots	C_1, C_3, C_5, C_7, C_9	$a_2, a_3, a_4, a_5, a_6,$ $a_7, 8, a_9, a_{10}$	$C_2, C_3, C_4, C_5, C_6,$ C_7, C_8, C_9, C_{10}
$B^0 \rightarrow a_2^0 \pi^0$	$a_2, a_4, a_6, a_7, a_8,$ a_9, a_{10}	$C_2, C_3, C_5, C_7, C_8,$ C_9, C_{10}	$a_2, a_3, a_4, a_5, a_6,$ $a_7, 8, a_9, a_{10}$	$C_2, C_3, C_4, C_5, C_6,$ C_7, C_8, C_9, C_{10}
$B^0 \rightarrow f_2^s \pi^0$	\dots	C_4, C_6, C_8, C_{10}	\dots	\dots
$B^0 \rightarrow \eta^s a_2^0$	a_3, a_5, a_7, a_9	C_4, C_6, C_8, C_{10}	\dots	\dots
$B^0 \rightarrow f_2^q \eta^q$	$a_2, a_3, a_4, a_5, a_6,$ a_7, a_8, a_9, a_{10}	$C_2, C_3, C_4, C_5, C_6,$ C_7, C_8, C_9, C_{10}	$a_2, a_3, a_4, a_5, a_6,$ a_7, a_8, a_9, a_{10}	$C_2, C_3, C_4, C_5, C_6,$ C_7, C_8, C_9, C_{10}
$B^0 \rightarrow f_2^s \eta^s$	\dots	\dots	a_3, a_5, a_7, a_9	C_4, C_6, C_8, C_{10}
$B^0 \rightarrow f_2^q \eta^s$	a_3, a_5, a_7, a_9	C_4, C_6, C_8, C_{10}	\dots	\dots
$B^0 \rightarrow f_2^s \eta^q$	\dots	C_4, C_6, C_8, C_{10}	\dots	\dots
$B^0 \rightarrow K_2^{*+} K^-$	\dots	\dots	a_2, a_3, a_5, a_7, a_9	$C_2, C_4, C_6, C_8, C_{10}$
$B^0 \rightarrow K_2^{*-} K^+$	\dots	\dots	a_2, a_3, a_5, a_7, a_9	$C_2, C_4, C_6, C_8, C_{10}$
$B^0 \rightarrow K_2^{*0} \bar{K}^0$	a_4, a_6, a_8, a_{10}	C_3, C_5, C_7, C_9	$a_3, a_4, a_5, a_6, a_7,$ a_8, a_9, a_{10}	$C_3, C_4, C_5, C_6, C_7,$ C_8, C_9, C_{10}
$B^0 \rightarrow \bar{K}_2^{*0} K^0$	\dots	C_3, C_5, C_7, C_9	$a_3, a_4, a_5, a_6, a_7,$ a_8, a_9, a_{10}	$C_3, C_4, C_5, C_6, C_7,$ C_8, C_9, C_{10}
$B^+ \rightarrow a_2^0 \pi^+$	$a_1, a_4, a_6, a_8, a_{10}$	$C_1, C_2, C_3, C_5, C_7,$ C_8, C_9, C_{10}	$a_1, a_4, a_6, a_8, a_{10}$	C_1, C_3, C_5, C_7, C_9
$B^+ \rightarrow a_2^+ \pi^0$	$a_2, a_4, a_6, a_7, a_8,$ a_9, a_{10}	$C_1, C_2, C_3, C_5, C_7,$ C_8, C_9, C_{10}	$a_1, a_4, a_6, a_8, a_{10}$	C_1, C_3, C_5, C_7, C_9
$B^+ \rightarrow f_2^q \pi^+$	$a_1, a_4, a_6, a_8, a_{10}$	$C_1, C_2, C_3, C_4, C_5,$ $C_6, C_7, C_8, C_9, C_{10}$	$a_1, a_4, a_6, a_8, a_{10}$	C_1, C_3, C_5, C_7, C_9
$B^+ \rightarrow \eta^q a_2^+$	$a_2, a_3, a_4, a_5, a_6,$ a_7, a_8, a_9, a_{10}	$C_1, C_2, C_3, C_4,$ $C_5, C_6, C_7, C_8, C_9, C_{10}$	$a_1, a_4, a_6, a_8, a_{10}$	C_1, C_3, C_5, C_7, C_9
$B^+ \rightarrow a_2^+ \eta^s$	a_3, a_5, a_7, a_9	C_4, C_6, C_8, C_{10}	\dots	\dots
$B^+ \rightarrow \pi^+ f_2^s$	\dots	C_4, C_6, C_8, C_{10}	\dots	\dots
$B^+ \rightarrow K^+ \bar{K}_2^{*0}$	\dots	C_3, C_5, C_7, C_9	$a_1, a_4, a_6, a_8, a_{10}$	C_1, C_3, C_5, C_7, C_9
$B^+ \rightarrow K_2^{*+} \bar{K}^0$	a_4, a_6, a_8, a_{10}	C_3, C_5, C_7, C_9	$a_1, a_4, a_6, a_8, a_{10}$	C_1, C_3, C_5, C_7, C_9

$$h_{anf1}(x_1, x_2, x_3, b_1, b_2) = \frac{i\pi}{2} [\theta(b_1 - b_2) H_0^{(1)}(\sqrt{x_2(1-x_3)} m_B b_1) J_0(\sqrt{x_2(1-x_3)} m_B b_2) + \theta(b_2 - b_1) H_0^{(1)}(\sqrt{x_2(1-x_3)} m_B b_2) J_0(\sqrt{x_2(1-x_3)} m_B b_1)] K_0(\sqrt{1 - (1-x_1-x_2)x_3} m_B b_1), \quad (\text{B17})$$

$$h_{anf2}(x_1, x_2, x_3, b_1, b_2) = \frac{i\pi}{2} [\theta(b_1 - b_2) H_0^{(1)}(\sqrt{x_2(1-x_3)} m_B b_1) J_0(\sqrt{x_2(1-x_3)} m_B b_2) + \theta(b_2 - b_1) H_0^{(1)}(\sqrt{x_2(1-x_3)} m_B b_2) J_0(\sqrt{x_2(1-x_3)} m_B b_1)] \times \begin{cases} \frac{i\pi}{2} H_0^{(1)}(\sqrt{(x_2-x_1)(1-x_3)} m_B b_1), & x_1 - x_2 < 0, \\ K_0(\sqrt{(x_1-x_2)(1-x_3)} m_B b_1), & x_1 - x_2 > 0, \end{cases} \quad (\text{B18})$$

where $H_0^{(1)}(z) = J_0(z) + iY_0(z)$.

- [1] K. Nakamura *et al.* (Particle Data Group), *J. Phys. G* **37**, 075021 (2010).
- [2] W. Wang, *Phys. Rev. D* **83**, 014008 (2011).
- [3] H.-Y. Cheng, Y. Koike, and K.-C. Yang, *Phys. Rev. D* **82**, 054019 (2010).
- [4] H.-Y. Cheng and K.-C. Yang, *Phys. Rev. D* **83**, 034001 (2011).
- [5] P. del Amo Sanchez *et al.* (BABAR Collaboration), *Phys. Rev. D* **82**, 011502 (2010).
- [6] B. Aubert *et al.* (BABAR Collaboration), *Phys. Rev. Lett.* **97**, 201802 (2006).
- [7] B. Aubert *et al.* (BABAR Collaboration), *Phys. Rev. D* **79**, 052005 (2009).
- [8] B. Aubert *et al.* (BABAR Collaboration), *Phys. Rev. D* **78**, 012004 (2008).
- [9] A. Garmash *et al.* (Belle Collaboration), *Phys. Rev. Lett.* **96**, 251803 (2006).
- [10] B. Aubert *et al.* (BABAR Collaboration), *Phys. Rev. D* **72**, 072003 (2005); **74**, 099903(E) (2006).
- [11] A. Garmash *et al.* (Belle Collaboration), *Phys. Rev. D* **71**, 092003 (2005).
- [12] Y. Unno (Belle Collaboration), *Nuovo Cimento Soc. Ital. Fis. C* **32**, 229 (2009).
- [13] B. Aubert *et al.* (BABAR Collaboration), *Phys. Rev. Lett.* **101**, 161801 (2008).
- [14] B. Aubert *et al.* (BABAR Collaboration), *Phys. Rev. D* **79**, 072006 (2009).
- [15] B. Aubert *et al.* (BABAR Collaboration), *Phys. Rev. D* **78**, 052005 (2008).
- [16] B. Aubert *et al.* (BABAR Collaboration), *Phys. Rev. D* **80**, 112001 (2009).
- [17] A. Garmash *et al.* (Belle Collaboration), *Phys. Rev. D* **75**, 012006 (2007).
- [18] B. Aubert *et al.* (BABAR Collaboration), *Phys. Rev. D* **78**, 092008 (2008).
- [19] A. C. Katoch and R. C. Verma, *Phys. Rev. D* **49**, 1645 (1994); **55**, 7315(E) (1997).
- [20] G. López Castro and J. H. Muñoz, *Phys. Rev. D* **55**, 5581 (1997).
- [21] J. H. Muñoz, A. A. Rojas, and G. López Castro, *Phys. Rev. D* **59**, 077504 (1999).
- [22] C. S. Kim, B. H. Lim, and S. Oh, *Eur. Phys. J. C* **22**, 683 (2002).
- [23] C. S. Kim, B. H. Lim, and S. Oh, *Eur. Phys. J. C* **22**, 695 (2002); **24**, 665(E) (2002).
- [24] C. S. Kim, B. H. Lim, and S. Oh, *Phys. Rev. D* **67**, 014002 (2003).
- [25] J. H. Muñoz and N. Quintero, *J. Phys. G* **36**, 095004 (2009).
- [26] N. Sharma and R. C. Verma, *Phys. Rev. D* **82**, 094014 (2010).
- [27] N. Sharma, R. Dhir, and R. C. Verma, *Phys. Rev. D* **83**, 014007 (2011).
- [28] Y. Y. Keum, H. N. Li, and A. I. Sanda, *Phys. Lett. B* **504**, 6 (2001); *Phys. Rev. D* **63**, 054008 (2001).
- [29] C.-D. Lü, K. Ukai, and M. Z. Yang, *Phys. Rev. D* **63**, 074009 (2001).
- [30] B. H. Hong and C.-D. Lü, *Sci. China: Phys., Mech. Astron.* **G49**, 357 (2006).
- [31] C.-D. Lü and K. Ukai, *Eur. Phys. J. C* **28**, 305 (2003); Y. Li and C.-D. Lü, *J. Phys. G* **29**, 2115 (2003); *High Energy Phys. Nucl. Phys.* **27**, 1062 (2003).
- [32] G. Buchalla, A. J. Buras, and M. E. Lautenbacher, *Rev. Mod. Phys.* **68**, 1125 (1996); A. J. Buras, arXiv:hep-ph/9806471.
- [33] H. N. Li, *Phys. Rev. D* **66**, 094010 (2002).
- [34] H. N. Li and B. Tseng, *Phys. Rev. D* **57**, 443 (1998).
- [35] C.-D. Lü and M. Z. Yang, *Eur. Phys. J. C* **23**, 275 (2002).
- [36] D. Asner *et al.* (Heavy Flavor Averaging Group), arXiv:1010.1589; online update at <http://www.slac.stanford.edu/xorg/hfag>.
- [37] T. Kurimoto, H. N. Li, and A. I. Sanda, *Phys. Rev. D* **65**, 014007 (2001); Z. T. Wei and M. Z. Yang, *Nucl. Phys. B* **642**, 263 (2002); C.-D. Lü and M. Z. Yang, *Eur. Phys. J. C* **28**, 515 (2003).
- [38] X. Liu, Z.-J. Xiao, and C.-D. Lü, *Phys. Rev. D* **81**, 014022 (2010).
- [39] Z.-J. Xiao, Z. Q. Zhang, X. Liu, and L. B. Guo, *Phys. Rev. D* **78**, 114001 (2008).
- [40] Z. Rui, G. Xiangdong, and C.-D. Lü, *Eur. Phys. J. C* **72**, 1923 (2012).
- [41] V. M. Braun and I. E. Filyanov, *Z. Phys. C* **48**, 239 (1990).
- [42] P. Ball, *J. High Energy Phys.* 01 (1999) 010.
- [43] Th. Feldmann, P. Kroll, and B. Stech, *Phys. Rev. D* **58**, 114006 (1998).
- [44] R. Escribano and J. M. Frere, *J. High Energy Phys.* 06 (2005) 029; J. Schechter, A. Subbaraman, and H. Weigel, *Phys. Rev. D* **48**, 339 (1993).
- [45] H.-Y. Cheng and R. Shrock, *Phys. Rev. D* **84**, 094008 (2011).
- [46] D. M. Li, H. Yu, and Q. X. Shen, *J. Phys. G* **27**, 807 (2001).
- [47] H. N. Li and K. Ukai, *Phys. Lett. B* **555**, 197 (2003).